Surfaces, Interfaces, and Applications

Tailoring the Tribocorrosion and Antifouling Performance of (Cr, Cu)-GLC Coatings for Marine Application

Xudong Sui, Rongnian Xu, Jian Liu, Shuaituo Zhang, Yang Wu, Jun Yang, and Junying Hao

ACS Appl. Mater. Interfaces, **Just Accepted Manuscript** • DOI: 10.1021/acsami.8b12359 • Publication Date (Web): 01 Oct 2018

Tailoring the Tribocorrosion and Antifouling Performance of (Cr, Cu)-GLC Coatings for Marine Application

Xudong Sui*[1,2], Rongnian Xu[1,3], Jian Liu[1,2], Shuaituo Zhang[1,2], Yang Wu[1,2], Jun Yang[1], Junying Hao*[1]

1: State Key Laboratory of Solid Lubrication, Lanzhou Institute of Chemical Physics, Chinese Academy of Science, Lanzhou 730000, China
2: Qingdao Center of Resource Chemistry and New Materials, Qingdao 266000, China
3: University of Chinese Academy of Sciences, Beijing 100049, China

* suixudong@licp.cas.cn; ** jyhao@licp.cas.cn

Abstract

Doped graphite-like coating (GLC) has aroused great interests as one of the promising protective material in marine application. However, there is a lack of systematic research on the tribocorrosion and antifouling performance of doped GLC coatings in harsh marine environments. Herein, a multi-functional (Cr, Cu)-GLC coating with combined antifouling and tribocorrosion properties was prepared via a magnetron sputtering method. The experimental results indicate that the resultant coatings changed from a dense structure to a loose columnar structure with the increment of Cr and Cu doping amount. At the same time, the hardness of the coating gradually decreases, but the contact angle between coating and seawater gradually increases. The algae adhesion test reveal that the algae density on the surface of the (Cr, Cu)-GLC coating decreases from about 565 to 70 /mm^2 as the amount of doping increased. However, on the contrary, the friction coefficient of the coating under OCP condition increases from 0.06 to about 0.35. Overall, the mild doped (Cr, Cu)-GLC coating exhibits the best comprehensive properties, combining antifouling and tribocorrosion properties. The corresponded mechanisms are discussed in terms of the coating microstructure, antifouling and tribocorrosion behavior.

Key words: GLC; Multi-doping; Tribocorrosion; Antifouling; Friction coefficient.

1. Introduction

Mechanical friction consumes a lot of resources and energy, and this situation is more serious and complicated in the marine environment.[1-3] One of the main reasons is that mechanical components will suffer electrochemical corrosion and friction wear at the same time under marine environment. This phenomenon is known as tribocorrosion and can cause severe loss of the metal components.[2, 4-6] In order to enhance the tribocorrosion performance of marine mechanical components, various method have been proposed. One of the popular strategies is to use surface function coatings with combined lubrication and anti-corrosion properties.[7-10]

Recently, amorphous carbon coatings have become a research hotspot in various applications due to their desirable mechanical and tribocorrosion properties. According to the content of sp^2 and sp^3 bonds, amorphous carbon coatings can be divided into graphite-like carbon (GLC) coating and diamond-like carbon (DLC).[11-13] As a member of amorphous carbon family, GLC coatings have been considered as potential candidates for use in the marine environment owing to its high hardness, low friction and chemical inertness.[2] Many studies have been conducted to investigate the tribological performance of GLC coatings in water environment. For example, Stallard et al.[14] demonstrated the Graphit-iC coatings exhibited better tribological performance than Dymon-iC coatings under water environment. Wang et al.[15] investigated the effect of interlayer design on the tribology properties of GLC coatings in seawater and found that the hard carbide phase and nano-interlocked microstructure were key to the tribological properties of GLC coatings in seawater. Recently, Li et al.[2] systematically studied the tribocorrosion properties of Cr/GLC multilayered coatings in seawater by a tribometer integrated with a three-electrode electrochemical system. They confirm the tribocorrosion resistacne of Cr/GLC multilayered coatings significantly depended on the modulation period.

In short, many studies have been conducted to investigate the tribocorrosion performance of GLC coatings in seawater environment. However, the application of mechanical components in the marine environment faces another great challenge-biofouling.[16-18] The attachment of marine organisms to the surface of mechanical components increases the frictional resistance, which not only affects the normal operation of marine equipment and increases energy consumption, but also easily causes microbial corrosion.[19,20] There have been many studies on antifouling and many papers have been published. For example, Secker et al.[21] demonstrated the doped DLC coatings significantly reduce the attachment of microbial and protein. Ivanov-Omskii et al.[22] reported that copper doped DLC coating can inhibit fungi growth at the coating surface. Liu et al.[23] also investigated copper doped DLC films in the simulated marine environment and found that copper doping can achieves anti-fouling by sustained release in seawater. However, little attention has been given to GLC coating. Furthermore, most research work only focuses on antifouling properties, and does not involve the tribocorrosion performance of the coating at the same time. There appears to be a lack of systematic study in the existing literature on the tribocorrosion and antifouling properties of GLC coatings.

For the above reasons, we want to fabricate a multi-functional doped GLC coating with both tribocorrosion and antifouling properties. According to previous study, the Cr and Cu elements were selected as doping elements because they can improve the corrosion resistance and antifouling properties of the coatings, respectively.[24-26] The influence of Cu and Cr doping on the microstructure, tribocorrosion and antifouling properties of the coatings was systematically investigated. The aim of the present work is to finally propose a new concept for the preparation of multifunctional (Cr, Cu)-GLC coating with excellent tribocorrosion and antifouling performance for marine application.

2. Experimental section

2.1 Sample preparation

The Cu and Cr doped GCL coatings were fabricated on AISI 440C steel (Φ 25 mm × 4 mm, Ra ≤ 0.05 μm) and silicon (100) substrates by DC magnetron sputtering method. The depositing system was

configured of one pure copper target (99.9%), one pure chromium target (99.9%) and two high pure graphite targets (99.999%). Before coating, the substrates were ultrasonically cleaned with acetone and alcohol for 10 minutes, respectively. The pre-treatment method are identical to those of our previous report.[27]

After the base pressure reached 1.0×10^{-3} Pa, all the samples were etched by Ar ions for 30 min by applying a negative bias voltage of 400 V. A pure Cr buffer layer was first deposited to improve the bond strength between the substrate and the GLC coating. Afterwards, the graphite targets were used to deposit GLC coatings and the Cr and Cu targets were controlled by triggering or turning off for doping. The doping amounts of (Cr, Cu)-GLC coating were tuned by the current of Cr and Cu targets. During the deposition process, a pulse negative bias of -60 V was applied to the samples. The detailed parameters of the coating preparation are shown in Table 1.

2.2 Coating characterization

The chemical composition of as-deposited coatings was characterized by X-ray photoelectron spectroscopy (XPS, Escalab 250). Scanning electron microscopy (SEM, Hitachi S-4800) was used to observe the morphologies and thickness of the coatings. An attached energy dispersive X-ray spectroscopy (EDS, Oxford) was used to analysis the composition of the worn coating surface. An atomic force microscope (AFM, NANOSURF C3000) was used to determine the surface morphologies of the coatings. The coating hardness was evaluated by a nanoindentation technique (AGILENT, Nano Indenter XP). In order to avoid the influence of the substrate on the coating hardness, the indentation depth is selected to be approximately 15% of the coating thickness. Five tests were conducted for each sample to obtain average values. Static water contact angle tests were used to evaluate the wetting transition of the coating on a video-based optical system (Dataphysics OCA20, Germany). A 5 μL artificial seawater was dropped onto the coating surface and the corresponding static water contact angle was measured. Five readings were conducted for each coating, and the mean values were recorded.

2.3 Antifouling testing

In this paper, adhered algae on four coatings with different content of Cr and Cu element were characterized by auto-fluorescence image analysis (Olympus, BX-51). Each samples were equilibrated in seawater prior to assay. Based on the instruction supported by Freshwater Algae Culture Collection at the Institute of Hydrobiology (http://algae.ihb.ac.cn/Default.aspx), green algae D. tertiolecta was cultured and used for settlement bioassay at 25 ^{o}C because they could breed in normal and maintain a high activity to interact with the substrate at this temperature. Typically, the coating sample was placed in a sterile water glass and 5 mL of algae suspension was added. After 24 h, before the characterization of attached algae count, the slides were washed slightly using artificial seawater three times to remove any loosely bound algae. A total of 10 measurement spots, each 0.14 mm^2, were taken on each wafers. The average percentage of settlement algae are calculated.

2.4 Tribocorrosion investigations

The tribocorrosion performance of the coatings was evaluated on a liner reciprocating tribometer integrated with a three electrode cell configuration (MFT-R4000, Lanzhou Institute of Chemical Physics, China). The schematic diagram of the tribocorrosion test is presented in Fig. 1. An Al_2O_3 ball (Φ 6 mm) was used as the counterpart for its high hardness and excellent corrosion resistance. The 3.5-wt% NaCl solution was chosen to simulate seawater environment. The tests were conducted at the normal load of 10 N, amplitude of 5 mm and frequency of 0.1 Hz. The coated samples were first stabilized in solution for about 15 minutes prior to loading. The open circuit potential (OCP) was measured for 5min before a 30-min sliding test was conducted. The OCP was continuously recorded until the end of the test. After the sliding, the corrosion and morphology of the wear tracks were investigated by SEM.

3. Results and discussion

3.1 Structure and morphology

The chemical composition of the coating was analysed by XPS and the results are shown in Table 2. In order to facilitate the subsequent discussion, the samples are numbered S1, S2, S3 and S4 respectively, depending on the amount of doping. Sample S1 is a Cr doped GLC coating for comparison. Samples S2,

S3 and S4 are the Cr and Cu multi-doped GLC coating, and the doping amount is gradually increased. The doped Cr and Cu elements are evenly distributed in the coating, which can be reflected in the EDX mapping results of the (Cr, Cu)-GLC coatings found in the Supporting Information (Figure S1). Fig. 2 presents the surface and cross-section morphologies of the as-deposited (Cr, Cu)-GLC coatings. The thickness of as-deposited coatings in this work is between 2.2 and 2.9 μm, and the thickness of the Cr buffer layer is controlled at about 150 nm. The structure of the Cr doped GLC coating (S1) is dense and has small particles on the surface. However, the Cr-Cu multi-doped GLC coatings exhibit a columnar structure with a loose surface morphology. As the amount of Cr-Cu doping increases, the columnar crystal size of the coating becomes larger, and the particle shape gradually changes from spherical to island-like. It is well known that there is a strong bond between Cr and C, whereas Cu and C are weakly bonded.[23,28,29] Therefore, as the amount of Cu doping increases, the Cu nanoclusters are more easily segregated from the amorphous carbon matrix to from two phase structures. To better probe changes in the surface morphology of the prepared coatings, AFM micrograph was employed as shown in Fig. 3. AFM images of the coatings are consistent with the SEM results. It can be clearly seen that the surface roughness of the coating gradually increases with the increment of Cr-Cu doped amount.

XPS technology is a reliable means to obtain surface information of materials. Fig. 4a shows the deconvoluted of Cu 2p core level spectra of the as-deposited (Cr, Cu)-GLC coatings. A strong Shake-up satellite is observed can be ascribed to the CuO, which absent for Cu_2O and metallic copper.[30] Therefore, two deconvoluted peaks of Cu $2p_{3/2}$ corresponding to Cu (931.9 eV) and CuO (933.7 eV). The presence of CuO phase into the coatings may be mainly caused by the deposition process or by the adsorption of oxygen in the air. In addition, with the increase of Cu doping amount, the CuO phase in the coating also shows an upward trend. Similar results were also found in the spectra of Cr $2p_{3/2}$ as shown in Fig. 4b. The left peak of Cu LM2 comes from the Auger spectra of Cu. The content of Cr_2O_3 phase also increases with the increment of Cr doping amount.

It is well known that the chemical states of carbon in the GLC coating has a large effect on the performance of the coating. Hence, we deconvoluted the C 1s spectra into three peaks around 284.4, 285.2 and 288.6 eV shown in Fig. 4c, which correspond to sp^3 carbon atoms, sp^2 carbon atoms and C=O contamination, respectively.[31,32] The obtained sp^2/sp^3 ratio of the coatings is present in Fig. 4d. It can be found that the sample S1 has the lowest sp^2/sp^3 ratio of 1.96. This means the content of sp^2 carbon atoms of the coating is about 66%, suggesting a GLC coating was deposited. As the doping amount increases, the sp^2/sp^3 ratio of the coatings peaks at 3.70 (sample S3), and then it decreases to 2.70 (sample S4).

3.2 Hardness and wettability

The hardness of the (Cr, Cu)-GLC coatings was evaluated, as shown in Fig. 5. It can be found the sample S1 has the highest hardness of about 17 GPa, which is higher than those GLC coatings (about 12 GPa) reported in the literatures.[33,34] This is mainly due to its dense structure and lowest sp^2/sp^3 ratio. As the amount of Cu and Cr doping increases, the hardness of the coating gradually decreases. The decrease in coating hardness is mainly due to the loosening of the coating structure by introduction of Cu nanoclusters into the matrix. In addition, the increase of sp^2/sp^3 ratio in the coating caused by doping can also result in a decrease of the coating hardness.[35] Fig. 6 shows the static contact angle between the (Cr, Cu)-GLC coatings and artificial seawater at room temperature. It can be clearly observed that the sample S1 (only Cr doped GLC coating) exhibited smallest contact angle of about 86.0°. However, after incorporating Cu into the GLC coatings, the contact angle of the sample S2 increased to about 91.8°. Continue to increase the doping amount of Cu and Cr, the contact angle of the coating gradually rises to about 96.2° of sample S4. According to the literatures, the wettability of the coating is related to the sp^2/sp^3 ratio.[36] Generally, as the amount of Cr doping increases, the proportion of sp^2 in the coating also increases.[37] The surface of the coating with a high sp^2 content has a lower number of dangling bonds. Therefore, the surface energy has less polar component and the hydrophobicity of the coating is increased.[38] In addition, as shown in Fig. 4 a and b, the oxides of Cu and Cr gradually increased with increasing doping amount. This also reduces the polar surface energy of the coatings, which reduces the

adsorption of polar molecules such as seawater.[38,39] Besides these, the wettability of the coating is also affected by its surface morphology. As shown in Fig. 2, the particle size and roughness of the coating increase obviously after doping with Cu and Cr. All of these factors lead to an increase in the hydrophobicity of the coating.

3.3 Antifouling and tribocorrosion properties

Fig. 7 presents the SLCM observation of the D. tertiolecta attached on the surface of the (Cr, Cu)-GLC coatings. Obviously, the amount of algae attached on the S1 coating with only Cr doping is the largest. After doping Cu into the coatings, the (Cr, Cu)-GLC coatings exhibited antifouling feature. The statistical algae density results are shown in Fig. 7e. It can be seen from the figure that the algae density of the coating is reduced from about 565 /mm^2 at S1 coating to 305 /mm^2 at S2 coating after incorporating Cu element. This is mainly due to the toxicity of copper ions, which can inhibit cell division and photosynthesis of algae.[40-42] As the amount of Cu and Cr doping increases, the algae density gradually decreases to about 70 /mm^2 at S4 coating, which is about eight times lower than S1 coating. Therefore, the (Cr, Cu)-GLC coatings with higher Cu content exhibited more pronounced antifouling performance. It will be appreciated that inhibition of bacterial adhesion and the toxicity of copper all contribute to improve the antifouling performance of the coating. But in this case, we believe that the toxic effects of Cu is more dominant. As we all known, copper has been widely used as an important antifouling agent for decades and is still widely used today.[26,43,44] The bactericidal ability of doping copper has also been demonstrated in diamond-like carbon based coating.[22] This is also the main reason for the choice of doping Cu in this work. In addition, as can be seen from Fig. 6 and 7, from S3 to S4 samples, the algae density on the surface of the coating is reduced by more than three times. However, the change in coating contact angle is not obvious, only increasing from about 95.1° to 96.2°. This indicates that the improvement of the antifouling ability of the (Cr, Cu)-GLC coating is mainly dominated by the bactericidal action mechanism of copper.

The friction coefficient curves of the (Cr, Cu)-GLC coatings as a function of time are displayed in Fig. 8 (bottom) along with their corresponding OCP results in Fig. 8 (top). In the initial soaking stage, as the amount of Cu and Cr doping increases, the OCP of (Cr, Cu)-GLC coating peaks at +0.075 V (S2 coating), and then gradually decreases to -0.002 V (S4 coating). The surface passivation layer is more easily formed in a high metal doped GLC coating, which helps to increase the OCP of the coating. However, too high metal doping can lose the coating surface and introduce open grain boundaries, resulting in a decrease of OCP.

When the load is applied, the tribocorrosion test was started. It can be found that no fluctuation in the OCP curve of the S1 coating and the friction coefficient of S1 coating is kept at a small value of about 0.06. This means that the S1 coating was not destroyed under current friction condition. Compared to the S1 coating, the friction coefficient of S2 coating fluctuates greatly at the beginning of the sliding. At the same time, the OCP of the S2 coating suddenly drops from to a lower value of -0.002 V. In this case, the changes of friction coefficient and OCP are mainly attributed to the removal of the passivation film in a rapid run-in period. After the transfer film is formed, the friction coefficient of the coating drops to about 0.08, tending to be stable. In short, the prepared S1 and S2 coatings exhibit excellent frictional performance in seawater. As shown in Fig. 9, blue columns represent the friction coefficient of our prepared S1 and S2 coatings, and columns of other colors represent the results reported in the references.[2,37,45-47] It can be found that the friction coefficient of the S1 and S2 coatings is less than 0.1, which is lower than the results reported in most literatures.

In the case of S3 and S4 coating, the coatings show a relatively high OCP, which is close to that of S2 coating. However, the coefficient of S3 and S4 coatings increased significantly. The change of the friction coefficient of S3 coating at the late stage of sliding is mainly due to its low hardness and the coating was quickly worn out. After the sliding stops, the OCP values of the S2, S3 and S4 coatings are all increased, suggesting that a passivation layer is formed on the surface.

3.4 Wear morphology and mechanisms

To better understand the tribocorrosion behavior of the coatings, SEM images of the wear track were taken as present in Fig. 10. It can be observed that the surface of the S1 coating has almost no wear, which is related to its high hardness and low friction coefficient in seawater. However, a careful look reveals that there are many tiny corrosion spots along the wear track of the S1 coating as shown in the enlarged vies of Fig. 10a. EDS results (point A in Tab. 3) show that these spots mainly contain C, Cr, Na and Cl. The XPS analysis of the wear track of the S1 coating after tribocorrosion test are provided as Supporting Information in Figure S2. Only the peaks of the coating elements were observed.

After copper is incorporated into the coating, the width of the wear track of the coating increased significantly. In the case of the S2 coating, the resultant wear track morphology is smooth with some shallow scratches as shown in Fig. 10b. There is no obvious spallation of the coating was found in the wear track, suggesting a good wear resistance of the S2 coating. In addition, the enlarged view in Fig. 10b shows that there are some black bonds in the wear scar, and EDS analysis (point B in Tab. 3) show that they mainly contain C, Cu, Cr and O. Therefore, the wear mechanism of the S2 coating can be classified as groove and adhesive wear.

Conversely, the S3 and S4 coatings experienced more severe wear after sliding. It can be clearly observed that there are coating flaking and a large amount of adhesion in the wear track. In addition, there are more wear debris and cracks on the edge of the wear track as shown in the enlarged view of Fig. 10c and d. Due to the loose columnar structure and low hardness of the S3 and S4 coatings, cracks are easily generated during sliding under a large load of 10 N in this test. At the same time, chloride ions are more likely to penetrate into the coating along the open grain boundaries, accelerating coating wear. Moreover, the wear track of both S3 and S4 coatings exhibited two colors under a secondary electronics detector. The middle white region of wear track (point D and F in Tab. 3) was found by EDS analysis to contain more than 75% Fe element, which can only come from the 440C substrate. This means that most of the coating in the middle of the wear track has worn out. The XPS analysis also found the Fe element in the wear track of the coating 3 (see Figure S3 in Supporting Information). The EDS results show that the gray

regions (point E and H in Tab. 3) on both sides of the wear track mainly contain C, Cr, Cu and O, suggesting an oxidative wear mechanism. In short, the S1 coating (Cr doped GLC) show the best tribological performance in artificial seawater. However, it has no effective antifouling ability of algae, and has a relatively low OCP value. After the incorporation of Cu, the coating achieves excellent antifouling properties. Moreover, this anti-fouling ability is multiplied as the amount of doping increases. Unfortunately, the coefficient of friction of the coating also increases as the amount of doping increases. On the whole, the S2 coating exhibits the best comprehensive properties, combining antifouling, corrosion resistance and tribological properties.

4. Conclusions

The (Cr, Cu)-GLC coatings have been developed by magnetron sputtering in this work. The resultant coatings changed from a dense structure to a loose columnar structure with the increment of Cr and Cu doping amount. At the same time, the particle shape gradually changes from spherical to island-like, resulting in a larger roughness. As the amount of Cu and Cr doping increases, the hardness of the coating gradually decreases, but the contact angle between coating and seawater gradually increases. The hardness is primarily controlled by the microstructure and the sp^2/sp^3 ratio of the coatings. The antifouling test revealed that the S4 coating with the highest doping amount has the best antifouling performance, which is about eight times higher than that of S1 coating. However, on the contrary, the tribological properties of the coating under OCP condition decreases as the amount of doping increases. In summary, the mild doped (Cr, Cu)-GLC coating shows the best comprehensive properties, combining antifouling, corrosion resistance and tribological properties.

Acknowledgments

The authors gratefully acknowledge the financial support of the National Key R&D Plan of China (No. 2018YFB0703803), National Natural Science Foundation of China (51805515, 51602317) and the CAS "Light of West China" Program.

Reference

1. Wood, R.J.K. Marine Wear and Tribocorrosion. Wear. 2017, 376, 893-910.

2. Li, L.; Liu, L. L.; Li, X. W.; Guo, P.; Ke, P. L.; Wang, A. Y. Enhanced Tribocorrosion Performance of Cr/GLC Multilayered Films for Marine Protective Application. ACS Appl. Mater. Interfaces 2018, 10, 13187-13198.

3. Wen, H. X.; Sun, J. J.; Chen, W. Tribological Study of the Key Friction Pairs Materials under Seawater: Status Quo and Prospects, Mater. Rev. 2016, 30, 85-91.

4. Celis, J. P.; Ponthiaux, P. Tribocorrosion, Wear, 2006, 261, 937-938.

5. Mischler, S. Triboelectrochemical Techniques and Interpretation Methods in Tribocorrosion: A Comparative Evaluation. Tribol. Int. 2008, 41, 573−583.

6. Wang, Z.; Chen, X. Y.; Gong, Y. F.; He, X. Y.; Wei, Y. K.; Li, H. Tribocorrosion Behaviours of Cold-Sprayed Diamond-Cu Composite Coatings in Artificial Sea Water. Surf. Eng. 2018, 34, 392-398.

7. Totolin, V.; Pejakovic, V.; Csanyi, T.; Hekele, O.; Huber, M.; Ripoll, M.R. Surface Engineering of Ti6Al4V Surfaces for Enhanced Tribocorrosion Performance in Artificial Seawater. Mater. Design 2016, 104, 10-18.

8. Khamseh, S.; Alibakhshi, E.; Mahdavian, M.; Saeb, M. R.; Vahabi, H.; Lecomte, J. S.; Laheurte, P. High-Performance Hybrid Coatings Based on Diamond-Like Carbon and Copper for Carbon Steel Protection. Diam. Relat. Mater. 2017, 80, 84-92.

9. Ye, Y. W.; Wang, Y. X.; Wang, C. T.; Li, J. L.; Yao, Y. R. An Analysis on Tribological Performance of CrCN Coatings with Different Carbon Contents in Seawater. Tribol. Int. 2015, 91, 131-139.

10. Chen, Q.; Cao, Y. Z.; Xie, Z. W.; Chen, T.; Wan, Y. Y.; Wang, H.; Chen, Y.; Zhou, Y. W.; Guo, Y. Y. Tribocorrosion Behaviors of CrN Coating in 3.5 wt% NaCl Solution. Thin Solid Films 2017, 622, 41-47.

11. Fan, X. Q.; Xue, Q. J. Wang, L. P. Carbon-Based Solid-Liquid Lubricating Coatings for Space Applications-A Review. Friction, 2015, 3, 191-207.

12. Robertson, J. Diamond-Like Amorphous Carbon. Mat. Sci. Eng. R. 2002, 37, 129-281.

13. Erdemir, A.; Donnet, C. Tribology of Diamond-Like Carbon Films: Recent Progress and Future Prospects, J. Phys. D 2006, 39, 311-327.

14. Stallard, J.; Mercs, D.; Jarratt, M.; Teer, D. G.; Shipway, P. H. A Study of the Tribological Behaviour of Three Carbon-Based Coatings, Tested in Air, Water and Oil Environments at High Loads. Surf. Coat. Technol. 2004, 177,545-551.

15. Wang, Y. X.; Pu, J. B.; Wang, J. F.; Li, J. L.; Chen, J. M.; Xue, Q. J. Interlayer Design for the Graphite-Like Carbon Film with High Load-Bearing Capacity under Sliding-Friction Condition in Water. Appl. Surf. Sci. 2014, 311, 816-824.

16. Yang, W. F.; Lin, P.; Cheng, D. C.; Zhang, L. Z.; Wu, Y.; Liu, Y. P.; Pei, X. W.; Zhou, F. Contribution of Charges in Polyvinyl Alcohol Networks to Marine Antifouling. ACS Appl. Mater. Interfaces 2017, 9, 18295-18304.

17. Al-Jumaili, A.; Alancherry, S.; Bazaka, K.; Jacob, M. V. Review on the Antimicrobial Properties of Carbon Nanostructures. Materials 2017, 10, 1066.

18. Su, X. J.; Zhao, Q.; Wang, S.; Bendavid, A. Modification of Diamond-Like Carbon Coatings with Fluorine to Reduce Biofouling Adhesion, Surf. Coat. Tech. 2010, 204, 2454-2458.

19. Chen, Z. F.; Zhao, W. J.; Mo, M. T.; Zhou, C. X.; Liu, G.; Zeng, Z. X.; Wu, X. D.; Xue, Q. J. Architecture of Modified Silica Resin Coatings with Various Micro/Nano Patterns for Fouling Resistance: Microstructure and Antifouling Performance. Rsc Adv. 2015, 5, 97862-97873.

20. Wang, Q.; Li, C. C.; Yan, X. F.; Zhang, Z. M.; Yu, L. M. Marine Antifouling Coating Technology with Low Surface Energy and Its Evaluation Methods. Mater. Rev. 2008, 22, 84-87.

21. Secker, T. J.; Herve, R.; Zhao, Q.; Borisenko, K. B.; Abel, E. W.; Keevil, C. W. Doped Diamond-Like Carbon Coatings for Surgical Instruments Reduce Protein and Prion-Amyloid Biofouling and Improve Subsequent Cleaning. Biofouling 2012, 28, 563-569.

22. Ivanov-Omskii, V. I.; Panina, L. K.; Yastrebov, S. G. Amorphous Hydrogenated Carbon Doped with Copper as Antifungal Protective Coating. Carbon, 2000, 38, 495-499.

23. Liu, Y.; Guo, P.; He, X. Y.; Li, L.; Wang, A. Y.; Li, H. Developing Transparent Copper-Doped Diamond-Like Carbon Films for Marine Antifouling Applications. Diam. Relat. Mater. 2016, 69, 144-151.

24. Mandal, P.; Ehiasarian, A. P.; Hovsepian, P. E. Lubricated Sliding Wear Mechanism of Chromium-doped Graphite-Like Carbon Coating. Tribol. Int. 2014, 77, 186-195.

25. Li, L.; Guo, P.; Liu, L. L.; Li, X. W.; Ke, P. L.; Wang, A. Y. Structural Design of Cr/GLC Films for High Tribological Performance in Artificial Seawater: Cr/GLC Ratio and Multilayer Structure. J. Mater. Sci. Technol. 2018, 34, 1273-1280.

26. Yebra, D. M.; Kill, S.; Dam-Johansen, K. Antifouling Technology - Past, Present and Future Steps Towards Efficient and Environmentally Friendly Antifouling Coatings. Prog. Org. Coat. 2004, 50, 75-104.

27. Sui, X. D.; Liu, J. Y.; Zhang, S. T.; Yang, J.; Hao, J. Y. Microstructure, Mechanical and Tribological Characterization of CrN/DLC/Cr-DLC Multilayer Coating with Improved Adhesive Wear Resistance. Appl. Surf. Sci. 2018, 439, 24-32.

28. Ha, P. C. T.; Mckenzie, D. R.; Bilek, M. M. M.; Kwok, S. C. H.; Chu, P. K.; Tay, B. K. Raman Spectroscopy Study of DLC Films Prepared by RF Plasma and Filtered Cathodic Arc. Surf. Coat. Tech. 2007, 201, 6734-6736.

29. Pal, S. K.; Jiang, J. C.; Meletis, E. I.; Effects of N-Doping on the Microstructure, Mechanical and Tribological Behavior of Cr-DLC Films. Surf. Coat. Tech. 2007, 201, 7917-7923.

30. Watts, J. F.; Wolstenholme, J. An Introduction to Surface Analysis by XPS and AES. Wiley-VCH, 2003, 224.

31. Qi, J. W.; Liu, H. T.; Luo, Y.; Zhang, D. K.; Wang, Y. X. Influences of Added Sand-Dust Particles on the Tribological Performance of Graphite-Like Coating under Solid-Liquid Lubrication. Tribol. Int. 2014, 71, 69-81.

32. Ahmed, S. F.; Alam, M. S.; Mukherjee, N. Cu Incorporated Amorphous Diamond Like Carbon (DLC) Composites: An Efficient Electron Field Emitter over A Wide Range of Temperature. Physica E 2018, 97, 120-125.

33. Huang, M. D.; Zhang, X. Q.; Ke, P. L.; Wang, A. Y. Graphite-Like Carbon Films by High Power Impulse Magnetron Sputtering. Appl. Surf. Sci. 2013, 283, 321-326.

34. Chen, J. M.; Wang, Y. J.; Li, H. X.; Ji, L.; Wu, Y. X.; Lv, Y. H.; Liu, X. H.; Fu, Y. Y.; Zhou, H. D. Microstructure, Morphology and Properties of Titanium Containing Graphite-Like Carbon Films Deposited by Unbalanced Magnetron Sputtering. Tribol. Int. 2013, 49, 47-59.

35. Hauert, R. A Review of Modified DLC Coatings for Biological Applications. Diam. Relat. Mater. 2003, 12, 583-589.

36. Ostrovskaya, L. Y.; Dementiev, A. P.; Kulakova, I. I.; Ralchenko, V. G. Chemical State and Wettability of Ion-Irradiated Diamond Surfaces. Diam. Relat. Mater. 2005, 14, 486-490.

37. Wang, Y. X.; Li, J. L.; Shan, L.; Chen, J. M.; Xue, Q. J. Tribological Performances of the Graphite-Like Carbon Films Deposited with Different Target Powers in Ambient Air and Distilled Water, Tribo. Int. 2014, 73, 17-24.

38. Sun, L. L.; Guo, P.; Ke, P. L.; Li, X. W.; Wang, A. Y. Synergistic Effect of Cu/Cr Co-Doping on the Wettability and Mechanical Properties of Diamond-Like Carbon Films. Diam. Relat. Mater. 2016, 68, 1-9.

39. Guo, P.; Sun, L. L.; Li, X. W.; Xu, S.; Ke, P. L.; Wang, A. Y. Structural Properties and Surface Wettability of Cu-Containing Diamond-Like Carbon Films Prepared by a Hybrid Linear Ion Beam Deposition Technique. Thin Solid Films 2015, 584, 289-293.

40. Voulvoulis, N.; Scrimshaw, M. D.; Lester, J. N. Alternative Antifouling Biocides. Appl. Organomet. Chem. 1999, 13, 135-143.

41. Stauber, J. L.; Florence, T. M. Mechanism of Toxicity of Ionic Copper and Copper Complexes to Algae. Mar. Biol. 1987, 94, 511-519.

42. Chan, Y. H.; Huang, C. F.; Ou, K. L.; Peng, P. W. Mechanical Properties and Antibacterial Activity of Copper Doped Diamond-Like Carbon Films. Surf. Coat. Tech. 2011, 206, 1037-1040.

43. Banerjee, I.; Pangule, R. C.; Kane, R. S. Antifouling Coatings: Recent Developments in the Design of Surfaces That Prevent Fouling by Proteins, Bacteria, and Marine Organisms. Adv. Mater. 2011, 23, 690-718.

44. Rubin, H. N.; Neufeld, B. H.; Reynolds, M. M. Surface-Anchored Metal-Organic Framework-Cotton Material for Tunable Antibacterial Copper Delivery. ACS Appl. Mater. Interfaces 2018, 10, 15189-15199.

45. Du, D.; Liu, D. X.; Ye, Z. Y.; Zhang, X. H.; Li, F. Q.; Zhou, Z. Q.; Yu, L. Fretting Wear and Fretting Fatigue Behaviors of Diamond-Like Carbon and Graphite-Like Carbon Films Deposited on Ti-6Al-4V Alloy. Appl. Surf. Sci. 2014, 313, 462-469.

46. Guan, X. Y.; Lu, Z. B.; Wang, L.P. Achieving High Tribological Performance of Graphite-Like Carbon Coatings on Ti6Al4V in Aqueous Environments by Gradient Interface Design. Tribol. Lett. 2011, 44, 315-325.

47. Ye, Y. W.; Wang, C. T.; Wang, Y. X.; Liu, W.; Liu, Z. Y.; Li, X. G. The Influence of Different Metallic Counterparts on the Tribological Performance of nc-CrC/GLC in Seawater. Surf. Coat. Tech. 2017, 325, 689-696.

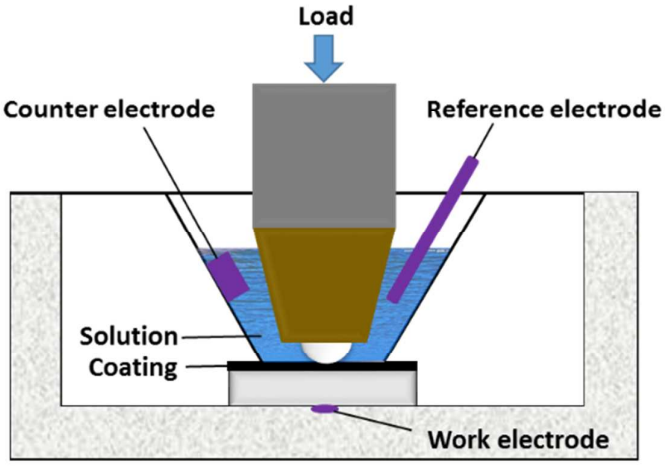

Fig. 1. The scheme diagram of the tribocorrosion test.

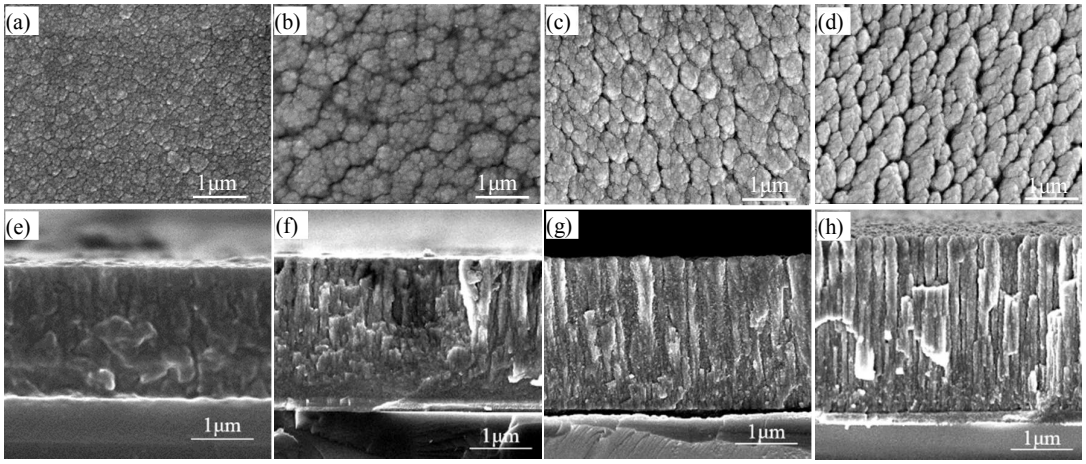

Fig. 2. SEM images of the coatings: (a-d) surface micrograph of S1 to S4 coatings and (e-h) cross-sectional micrograph of S1 to S4 coatings.

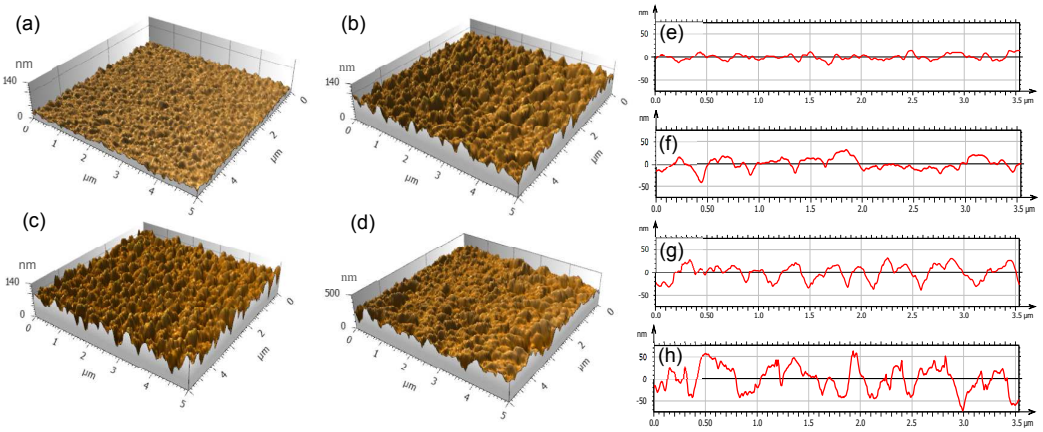

Fig. 3. AFM results of the coatings: (a-d) AFM images of S1 to S4 coatings and (e-h) line roughness of S1 to S4 coatings.

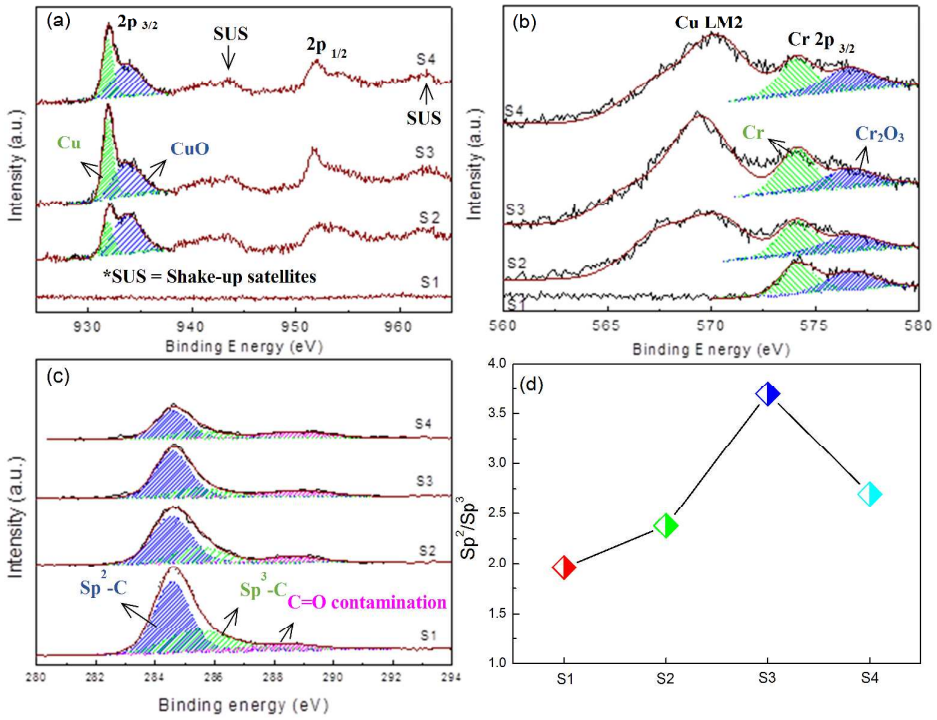

Fig. 4. Deconvoluted XPS spectrum of the Cu 2p (a), Cr 2p (b) and C 1s (c); (d) the calculated sp^2/sp^3 ratio from C 1s spectrum.

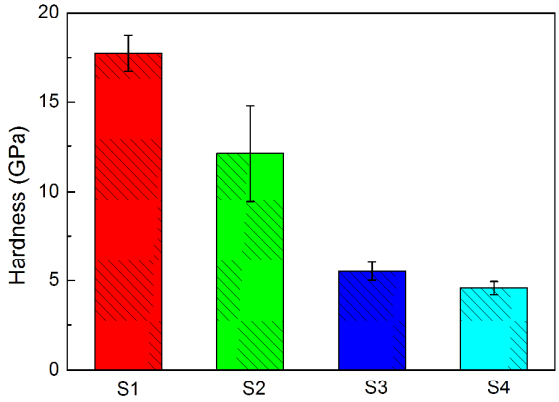

Fig. 5. Hardness of the (Cr, Cu)-GLC coatings.

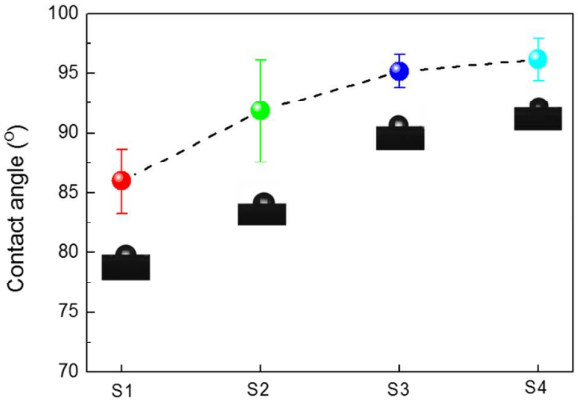

Fig. 6. Static contact angle between the (Cr, Cu)-GLC coatings and artificial seawater

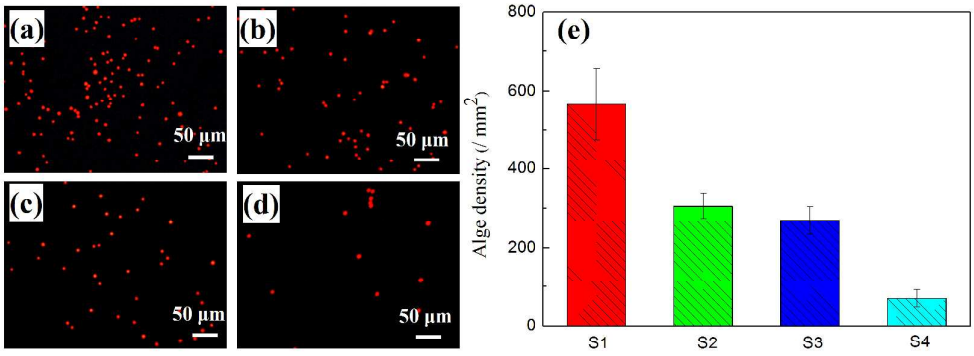

Fig. 7. SLCM images showing adhesion of D. tertiolecta on the surface of (a-d) S1 to S4 coatings. (e) the algae cell density of D. tertiolecta. D. tertiolecta was counted by optical microscope at 20× magnification and each value is the average of ten measurements.

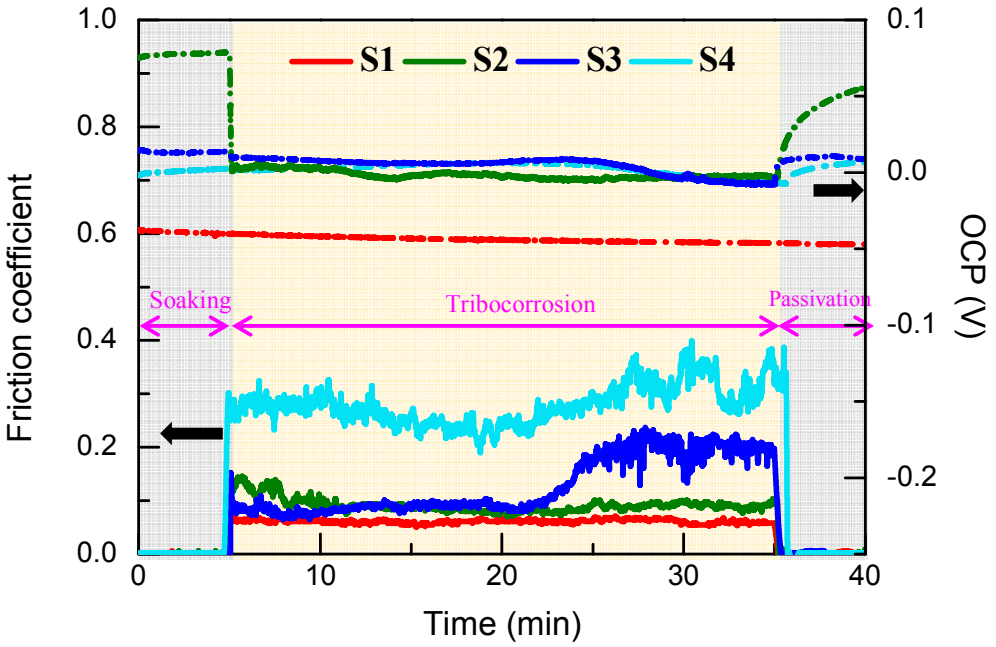

Fig. 8. Tribocorrsosion results of (Cr, Cu)-GLC coatings.

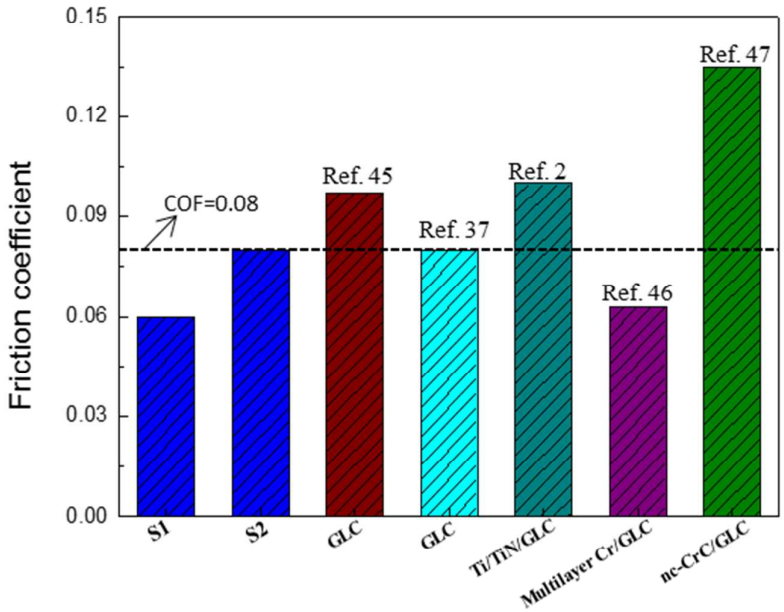

Fig. 9. Comparison of the friction coefficient of the as-deposited coatings and the reported GLC coatings.

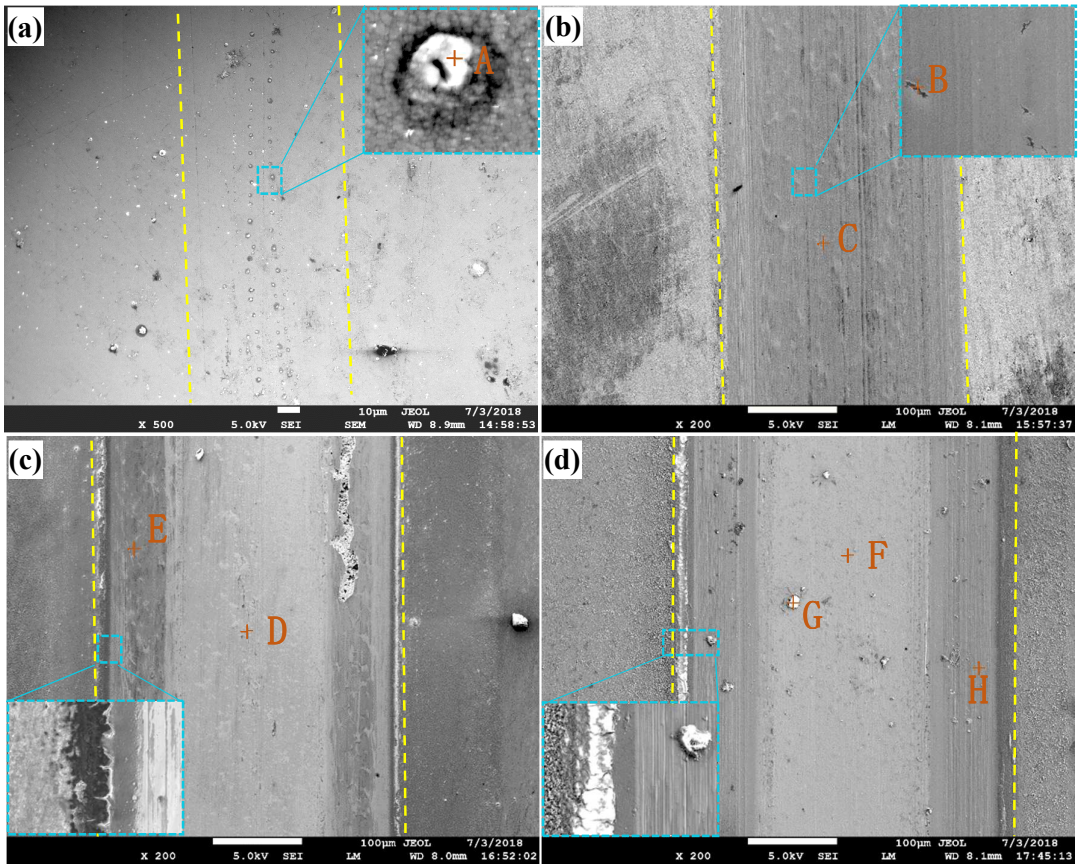

Fig. 10. SEM images of wear tracks of the (Cr, Cu)-GLC coatings. (a) S1, (b) S2, (c) S3, and (d) S4.

Table 1 Deposition parameters for the coatings

Coatings	S1		S2		S3		S4	
	Cr	Cr-GLC	Cr	(Cu,Cr)-GLC	Cr	(Cu,Cr)-GLC	Cr	(Cu,Cr)-GLC
Cr target power (DC, A)	4	0.5	4	0.5	4	1.0	4	1.5
Cu target power (DC, A)	–	–	–	0.5	–	1.0	–	1.5
C target power (DC, A)	–	3.5	–	3.5	–	3.5	–	3.5
Bias voltage (V)	-60	-60	-60	-60	-60	-60	-60	-60
Pressure (Pa)	1	1	1	1	1	1	1	1
Ar flow rate (sccm)	20	20	20	20	20	20	20	20
Deposition time (min)	5	400	5	280	5	167	5	125

Table 2 the chemical composition of the (Cr, Cu)-GLC coatings

Sample	C (at. %)	Cr (at. %)	Cu (at. %)
S1	96.46	3.54	—
S2	83.24	4.29	12.47
S3	77.01	6.23	16.76
S4	73.00	6.99	20.01

Table 3 EDS results of the different coatings after tribocorrosion test

Point	C (at. %)	Cr (at. %)	Cu (at. %)	Fe (at. %)	Na (at. %)	Cl (at. %)	O (at. %)
A	70.34	19.96	--	--	6.85	2.85	–
B	42.34	10.60	25.41	--	--	--	21.65
C	46.80	13.25	31.44	--	--	–	8.51
D	7.06	15.82	--	75.47	--	–	1.65
E	29.97	19.26	34.13	2.87	--	--	13.77
F	5.73	13.58	--	78.85	--	--	1.84
G	13.06	1.27	7.61	0.72	20.40	13.83	43.11
H	12.10	13.73	8.62	2.00	7.06	0.34	56.15

Table of contents